PROTEINS: Structure, Function, and Bioinformatics 65:000–000 (2006)

Two Alternative Substrate Paths for Compound I Formation and Reduction in Catalase–Peroxidase KatG From *Burkholderia pseudomallei*

Taweewat Deemagarn,[1] Ben Wiseman,[1] Xavier Carpena,[2] Anabella Ivancich,[3] Ignacio Fita,[2] and Peter C. Loewen[1]*

[1]*Department of Microbiology, University of Manitoba, Winnipeg, Manitoba R3T 2N2, Canada*
[2]*Departament de Biologia Estructural (IBMB-CSIC), Institut de Recerca Biomedica (IRB), Parc Científic de Barcelona, 08028 Barcelona, Spain*
[3]*Service de Bioénergétique, URA 2096 CNRS, Département de Biologie Joliot-Curie, CEA Saclay, 91191 Gif-sur-Yvette, France*

ABSTRACT **Five residues in the multifunctional catalase–peroxidase KatG of *Burkholderia pesudomallei* are essential for catalase, but not peroxidase, activity. Asp141 is the only one of these catalase-specific residues not related with the covalent adduct found in KatGs that when replaced with a nonacidic residue reduces catalase activity to 5% of native levels. Replacing the nearby catalytic residue Arg108 causes a reduction in catalase activity to 35% of native levels, whereas a variant with both Asp141 and Arg108 replaced exhibits near normal catalase activity (82% of native), suggesting a synergism in the roles of the two residues in support of catalase activity in the enzyme. Among the Asp141 variants, D141E is unique in retaining normal catalase activity but with modified kinetics, suggesting more favorable compound I formation and less favorable compound I reduction. The crystal structure of the D141E variant has been determined at 1.8-Å resolution, revealing that the carboxylate of Glu141 is moved only slightly compared with Asp141, but retains its hydrogen bond interaction with the main chain nitrogen of Ile237. In contrast, the low temperature ferric electron paramagnetic resonance spectra of the D141A, R108A, and R108A/D141A variants are consistent with modifications of the water matrix and/or the relative positioning of the distal residue side chains. Such changes explain the reduction in catalase activity in all but the double variant R108A/D141A. Two pathways of hydrogen bonded solvent lead from the entrance channel into the heme active site, one running between Asp141 and Arg108 and the second between Asp141 and the main chain atoms of residues 237–239. It is proposed that binding of substrate H_2O_2 to Asp141 and Arg108 controls H_2O_2 access to the heme active site, thereby modulating the catalase reaction. Proteins 2006;65:000–000.**

Key words: catalase; peroxidase; KatG; crystal structure; electron paramagnetic resonance

INTRODUCTION

Catalase–peroxidases or KatGs found primarily in bacteria, archaebacteria, and a few fungi are proving to be even more complex than their hybrid name suggests.[1] Named for the predominant catalase and peroxidase activities, additional low levels of NADH oxidase, INH lyase, and isonicotinoyl-NAD synthase activities have recently been characterized.[2] Isonicotinoyl-NAD is the activated form of the prodrug isoniazid and its production by KatG makes the enzyme responsible for the activation of INH as an antitubercular drug in *Mycobacterium tuberculosis*.[3–7]

The predominant catalase and peroxidase reactions involve a common path for compound I formation (Reaction 1), but differ in the path for compound I reduction back to resting state. Of the two electrons transferred to the oxygen during compound I formation, one is from the iron ($Fe^{III} \rightarrow Fe^{IV} = O$) and the second is from the porphyrin generating a porphyrin cation radical (Reaction 1). In some cases, there is a further intramolecular electron transfer from a tyrosine or tryptophan residue (Reaction 2). KatG from *Synechocystis* PCC6803 has been characterized as forming a $Por^{\bullet+}$-$Fe^{IV} = O$ intermediate and subsequent $Trp^{\bullet}$ and $Tyr^{\bullet}$ intermediates in the absence of H_2O_2 or peroxidase substrate (Reaction 2).[8] A single two-electron transfer from H_2O_2 (Reaction 3) is employed by catalases, whereas two consecutive one-electron transfers, usually from organic donors and involving a hydroxoferryl intermediate called compound II, are employed by peroxidases (Reactions 4 and 5).

The Supplementary Material referred to in this article can be found at http://www.interscience.wiley.com/jpages/0887-3585/suppmat/

Grant sponsor: Natural Sciences and Engineering Research Council of Canada; Grant number: OGP9600; Grant sponsor: Canadian Research Chair Program; Grant sponsor: Ministerio de Educacion y Ciencia of Spain; Grant number: BFU2005-08686-C02-01.

*Correspondence to: Peter C. Loewen, Department of Microbiology, University of Manitoba, Winnipeg, MB R3T 2N2, Canada. E-mail: peter_loewen@umanitoba.ca

Received 22 June 2006; Revised 21 July 2006; Accepted 14 August 2006

Published online 00 Month 2006 in Wiley InterScience (www.interscience.wiley.com). DOI: 10.1002/prot.21209

J_ID: Z7E Customer A_ID: 21209 Cadmus Art: PROT21209 Date: 2-OCTOBER-06 Stage: I Page: 2

$$\text{Enz (Por-Fe}^{\text{III}}) + H_2O_2 \rightarrow \text{Cpd I (Por}^{\bullet+}\text{-Fe}^{\text{IV}} = O) + H_2O \quad (1)$$

$$\text{Cpd I (Por}^{\bullet+}\text{-Fe}^{\text{IV}} = O) \rightarrow \text{CpdI (Por-Fe}^{\text{IV}}\text{-OH Trp}^{\bullet}) \rightarrow \text{CpdI (Por-Fe}^{\text{IV}}\text{-OH Tyr}^{\bullet}) \quad (2)$$

$$\text{Cpd I (Por}^{\bullet+}\text{-Fe}^{\text{IV}} = O) + H_2O_2 \rightarrow \text{Enz (Por-Fe}^{\text{III}}) + H_2O + O_2 \quad (3)$$

$$\text{Cpd I (Por}^{\bullet+}\text{/Trp}^{\bullet}\text{/Tyr}^{\bullet}\text{-Fe}^{\text{IV}}\text{-OH}) + AH \rightarrow \text{CpdII (Por/Trp/Tyr-Fe}^{\text{IV}}\text{-OH}) + A_{ox} \quad (4)$$

$$\text{CpdII (Por/Trp/Tyr-Fe}^{\text{IV}}\text{-OH}) + AH \rightarrow \text{Enz(Por-Fe}^{\text{III}}) + H_2O + A_{ox} \quad (5)$$

The predominant quaternary structure of KatGs is a dimer in which each subunit has two distinct, but sequence-related, domains that are similar in sequence and structure to plant peroxidases. Evolution of KatGs appears to have involved a gene duplication and fusion event,[9] which was subsequently reversed to produce the sequence-related, single-domain subunit plant peroxidases later in evolution. Specific features imparting catalase activity were also lost at this time.[1]

The identification of catalase-specific features in KatGs has been the focus of several recent structure–function studies aided by the recently reported crystal structures of catalase–peroxidases from *Haloarcula marismortui*,[10] *Burkholderia pseudomallei*,[11] *Synecococcus* sp.,[12] and *Mycobacterium tuberculosis*.[13] Of the invariant active site residues on the distal side of the heme, Arg108 and His112 (numbering in *B. pseudomallei* KatG, BpKatG, is used throughout), are also invariant and in a similar spatial arrangement relative to the heme in cytochrome c peroxidase (CcP). This suggested a possible catalase-specific role for other residues such as Trp111 and Asp141 which was first confirmed for Trp111[14,15] and extended to the adjacent Tyr238 and Met264, all three of which are joined in an unusual crosslinked adduct of Met-Tyr-Trp found in all catalase–peroxidases.[10–13,16] Similar to the changes to Trp111, changes to either Tyr238 or Met264, or to Arg426 associated with Tyr238, inhibited the catalase reaction with little or no effect on the peroxidase reaction.[2,17–19] A molecular mechanism by which these four residues control catalase activity has been proposed.[20]

Asp141 is unlinked to the Met-Tyr-Trp adduct, but changes to it also significantly reduce catalase activity with little effect on peroxidase activity.[2,21] Asp141 is situated in the heme distal cavity at the main access channel entrance, with its C^{α} atom about 10.0 Å from the heme iron (see Fig. 1), and proposals for its role in the catalytic mechanism have included catalytic proton extraction from the substrate and creation of an electrical potential field orienting substrate dipoles.[21,22] Involvement of Asp141 in the catalase reaction has been revisited in this report because of its apparent independence from the catalytic mechanism involving the molecular switch of Arg426.[20] The crystal structure of the D141E variant is reported and correlated with the 9-GHz electron paramagnetic resonance (EPR) spectrum of the ferric enzyme. In addition, the EPR spectra of other Asp141 and Arg108 variants allowed the inference of structural changes induced by the mutations. The restoration of catalase activity in a variant lacking both Arg108 and Asp141 provides new insights into the role of both residues in the control of substrate access to the active site.

MATERIALS AND METHODS

The variants of BpKatG were constructed, purified from the catalase-deficient *E. coli* strain UM262, and crystallized as previously described for other variants.[11,16] For pH change, a crystal was soaked for 1 min in 20% PEG 4K, 20% MPD, and 100 m*M* Tris-HCl at pH 8.0 before flash cooling for data collection. Diffraction data were obtained from crystals cooled with a nitrogen cryostream. As before, crystals were primitive orthorhombic space group $P2_12_12_1$ with one dimeric molecule in the crystal asymmetric unit. The diffraction data sets were processed using the program DENZO and scaled with program SCALEPACK.[23] Five percent of the measured reflections in every data set were reserved for R_{free} monitoring during automatic refinement (Table I). The resulting map showed clear continuity over the complete length from Asn35 to Ala748 in both subunits. Refinement was completed using the program REFMAC[24] and the graphics program O.[25] Figures were prepared using SETOR[26] or VMD.[27]

Low temperature (4 K) 9-GHz EPR measurements were performed using a Bruker ER 300 spectrometer with a standard TE_{102} cavity equipped with a liquid helium cryostat (Oxford Instrument) and a microwave frequency counter (Hewlett Packard 5350B). Samples were prepared by buffer exchange using Centricon 10 microconcentrators (Amicon) and 20 m*M* Tris-maleate buffer for pH 5.6 and 8.0. EPR samples were measured as frozen solutions in 4-mm quartz tubes.

Catalase activity was determined by the method of Rørth and Jensen[28] in a Gilson oxygraph equipped with a Clark electrode. One unit of catalase is defined as the amount that decomposes 1 μmol of H_2O_2 in 1 min in a 60 m*M* H_2O_2 solution at pH 7.0 and 37°C. Peroxidase activity was determined using ABTS (2,2′-azinobis(3-ethylbenzothiazolinesulfonic acid)).[29] One unit of peroxidase is defined as the amount that decomposes 1 μmol of ABTS in 1 min in a solution of 0.3 m*M* ABTS (ε = 36,800 M^{-1} cm^{-1}) and 2.5 m*M* H_2O_2 at pH 4.5 and

J_ID: Z7E Customer A_ID: 21209 Cadmus Art: PROT21209 Date: 2-OCTOBER-06 Stage: I Page: 3

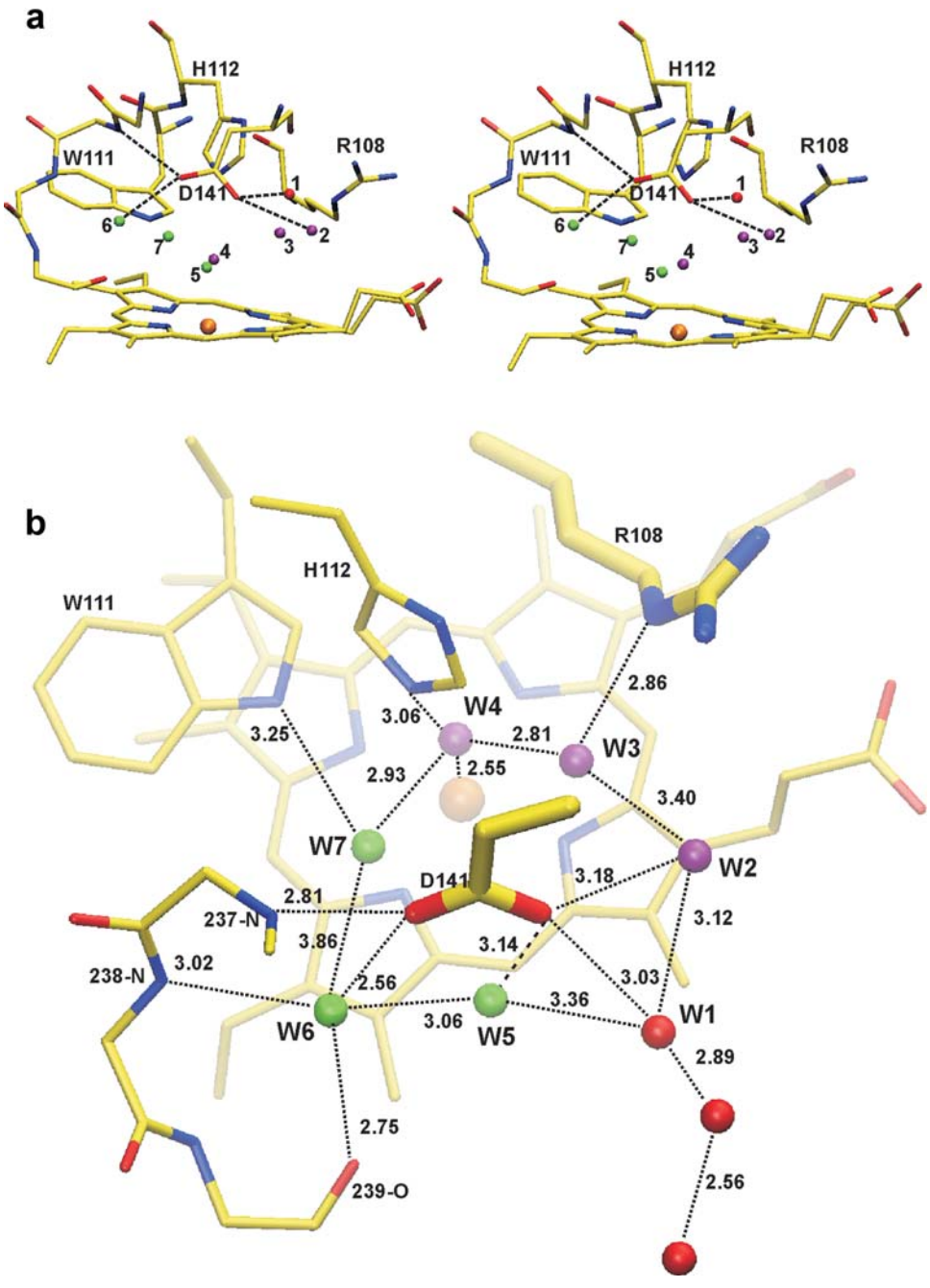

Fig. 1. (**a**) Stereo view of the atoms in the heme cavity of native BpKatG. The hydrogen bond interactions of Asp141 with the main chain nitrogen of Ile237 and adjacent waters are shown with dashed lines. The two chains of waters leading into the heme cavity are distinguished by color with the waters in the path leading beside Asp141 and Arg108 colored purple and the waters in the path leading beside Asp141 and residues 237–239 colored green. (**b**) Diagram showing the solvent molecules in the heme cavity and their hydrogen bond interactions. The diagram is rotated approximately 90° compared with the diagrams in panel (a) and the view is from the top. Waters colored red are situated in the main part of the entrance channel and the division at Asp141 is illustrated with waters colored purple passing by Arg108 and waters colored green passing by the main chain atoms of residues 237–239. Only waters involved in the paths leading to the heme iron are shown.

C O L O R

25°C. Protein concentration was estimated according to the methods outlined by Layne.[30]

Structure factors and coordinates have been submitted to the Protein Data Bank under accession numbers XXX (D141E at pH 5.6) and YYY (D141E at pH 8.0).

RESULTS

Effect of Changes in Arg108 and Asp141 on Enzyme Activity

Variants of residue 141 in BpKatG lacking an acidic side chain (D141A and D141N) exhibit reduced turn

J_ID: Z7E Customer A_ID: 21209 Cadmus Art: PROT21209 Date: 2-OCTOBER-06 Stage: I Page: 4

TABLE I. Data Collection and Structural Refinement Statistics for the D141E Variant of BpKatG

	pH 5.6	pH 8.0
Data collection statistics		
Unit cell parameters		
Space group	$P2_12_12_1$	$P2_12_12_1$
a, b, c (Å)	100.7, 116.2, 175.0	100.3, 114.8, 174.3
α, β, γ (°)	90, 90, 90	90, 90, 90
Resolution (Å)	30–1.8 (1.86–1.80)[a]	30–2.15 (2.15–2.20)
Unique reflections	188,800 (17,899)	108,948 (10,483)
Completeness (%)	99.1 (94.9)	99.1 (96.7)
R_{sym} (%)[b]	10.8 (43.3)	9.6 (44.7)
$<I/\sigma I>$	9.3 (3.1)	13.9 (44.7)
Redundancy	5.7 (4.4)	4.9 (4.6)
Model refinement statistics		
Resolution	30–1.8 (1.85–1.80)	30–2.1 (2.15–2.10)
Number of reflections	178,806 (12,325)	103,428 (7270)
Free reflections	9433 (683)	5450 (365)
R_{cryst} (%)[c]	16.4 (23.3)	14.7 (18.9)
R_{free} (%)[d]	19.6 (28.1)	18.2 (22.5)
Number of residues	1428	1428
Number of waters	1383	1393
Average B-factor (Å^2)		
Protein	20.3	23.3
Water	29.3	32.7
All atoms	21.3	25.8
RMSD		
Bond lengths (Å)	0.027	0.018
Bond angles (°)	2.05	1.53

[a]Values in parentheses correspond to the highest resolution shell.
[b]$R_{sym} = E_{hkl}\, E_j\, |I_{hkl,j} - <I_{hkl}>| / E_{hkl} <I_{hkl}>$, where j extends to all the observed hkl symmetry related reflections.
[c]$R_{cryst} = \Sigma ||F_{obs}| - |F_{calc}|| / \Sigma |F_{obs}|$.
[d]R_{free} is as for R_{cryst} but calculated for a test set comprising reflections not used in the refinement.

over rates with only a small reduction in peroxidase reaction rate (Table II). More significantly in terms of the reaction pathway, replacement of Asp141 lowers the apparent K_m for H_2O_2 for compound I formation (evident in the peroxidase kinetic constants in Table II), and greatly increases the apparent K_m for H_2O_2 for compound I reduction in the catalase reaction (catalase kinetic constants in Table II and Ref. 2), closely reflecting the properties of similar variants of SyKatG.[21,22] These data confirm that Asp141, in native BpKatG, has the contradictory effects of hindering H_2O_2 binding for compound I formation (the peroxidatic K_m for H_2O_2 is lower in the absence of Asp141, 90–190 μ*M* compared with 310 μ*M*) and facilitating the H_2O_2 binding for catalatic compound I reduction (the catalatic K_m for H_2O_2 is lower in the presence of Asp141, 3.7 m*M* compared with 60–95 m*M*). The position of Asp141 in the entrance channel does not allow direct interaction with the heme iron, but the positioning of its carboxylate just 5.7 Å from the guanidinium side chain of Arg108 (see Fig. 1) suggests that its role may lie in modulating the entry of substrate into the active site, working in concert with Arg108. This was investigated in a variant lacking both Arg108 and Asp141, R108A/D141A, which retains 82% of the native catalase turn over rate, in sharp contrast to the individual variants, R108A and D141A, which exhibit 35 and 5%, respectively, of native catalase turn-over rates (Table II). This result clearly demonstrates a mutual dependence of the two residues with Asp141 being essential for catalase activity only when Arg108 is present and Arg108 having its greatest influence on the catalase reaction in the presence of Asp141. It should be noted that the catalase reaction of BpKatG and its variants differ from monofunctional catalases in following Michaelis–Menten kinetics closely, possibly a reflection of the lower H_2O_2 concentrations involved and in not being inhibited by H_2O_2 concentrations up to 1*M*.

In cytochrome c peroxidase (CcP), the distal side Arg is essential for compound I formation with the R48A variant exhibiting only 5% of native activity.[31] By analogy with peroxidases, Arg108 in KatGs has been ascribed the role of binding H_2O_2 in conjunction with His112 for compound I formation, but a significant level of activity, 35% of native catalase and 60% of native peroxidase, is retained in the R108A variant (Table II). There is a corresponding increase in the K_m for H_2O_2 in the peroxidase reaction (from 310 to 500 μ*M*) consistent with Arg108 having a role in compound I formation, but it is clear that its role can be satisfied reasonably well by another residue. The most likely candidate is Trp111,

J_ID: Z7E Customer A_ID: 21209 Cadmus Art: PROT21209 Date: 2-OCTOBER-06 Stage: I Page: 5

TABLE II. Kinetic Constants for Catalase and Peroxidase Activities of BpKatG and its Variants

	Catalase				Peroxidase				
					K_m(app)				
	V_{max} [a]	K_m [b](app)	k_{cat} (s^{-1})	k_{cat}/K_m [c]	V_{max} [d]	$[H_2O_2]$ (μM)	[ABTS] (μM)	k_{cat} (s^{-1})	k_{cat}/K_m [c]
BpKatG	4300 ± 300	3.7 ± 0.9	5680 ± 400	1.5×10^6	10.9 ± 1.4	310 ± 13	140 ± 5	14.4 ± 1.8	4.6×10^4
R108A	1480 ± 40	13 ± 1.6	1950 ± 50	1.5×10^5	6.2 ± 0.2	500 ± 50	410 ± 36	8.2 ± 0.3	1.6×10^4
R108K	1600 ± 120	180 ± 20	2110 ± 150	1.2×10^4	2.9 ± 0.2	980 ± 90	550 ± 170	3.8 ± 0.9	3.9×10^3
D141A	200 ± 15	60 ± 4.7	265 ± 20	4.4×10^3	6.2 ± 0.2	190 ± 20	30 ± 6.0	8.2 ± 0.3	4.3×10^4
D141N	900 ± 90	95 ± 24	1190 ± 120	1.3×10^4	7.4 ± 0.2	90 ± 15	9.2 ± 1.3	9.8 ± 0.3	1.1×10^5
D141E	4650 ± 360	75 ± 16	6140 ± 480	8.2×10^4	5.5 ± 0.3	120 ± 15	70 ± 19	7.3 ± 0.4	6.1×10^4
R108A/D141A	3500 ± 110	32 ± 4.0	4620 ± 145	1.4×10^5	4.5 ± 0.1	270 ± 30	78 ± 6.9	5.9 ± 0.1	2.2×10^4
R108A/W111F	26 ± 0.8	36 ± 4.7	34 ± 1.1	0.9×10^3	0.2 ± 0.006	560 ± 160	24 ± 5.9	0.22 ± 0.008	3.9×10^2
R108A/W111F/D141A	24 ± 0.9	35 ± 5.4	32 ± 1.2	0.9×10^3	0.2 ± 0.004	920 ± 220	5.5 ± 0.7	0.29 ± 0.005	3.2×10^2

[a] V_{max}, μM H_2O_2 min^{-1} mg^{-1} observed.
[b] K_m(app), $[H_2O_2]$ at 0.5 V_{max}, mM.
[c] k_{cat}/K_m, s^{-1} M^{-1} in terms of $[H_2O_2]$ for both the catalase and peroxidase reactions.
[d] V_{max}, mM ABTS min^{-1} mg^{-1}.

previously implicated in the binding of H_2O_2 in conjunction with His112 for compound I reduction, and the loss of all catalase and peroxidase activity when a mutation in Trp111 is introduced into the double and triple variants R108A/W111F and R108A/W111F/D141A (Table II) confirms this surmise. Thus, Trp111 can have a catalytic role in compound I formation, albeit less efficient than Arg108, as well as in compound I reduction.

Crystal Structure of the D141E Variant

Not all variants of BpKatG have proved to be amenable to crystallization, particularly those variants that have a significant effect on catalase activity. The S324T variant proved to be one key exception, but it retains normal catalase and peroxidase activity. Variant D141A proved to be similar to other inactive variants in not generating crystals, but variant D141E did crystallize under the same conditions as the native enzyme, and the crystals diffracted to 1.8-Å resolution (Table I). The electron density maps define main chain and side chain atoms of 1426 amino acids, two metal ions, two heme groups, and 1383 waters in two subunits. As in the native enzyme, the 34 N-terminal residues are not visible, but the maps show clear continuity from Asn35 to Ala748 in two subunits. There are two regions showing divergence from the structure of the native enzyme. The first is in the neighborhood of residue 141 and the second is in the location of the side chain of Arg426.

The electron density maps in the vicinity of residue 141 in both subunits are best satisfied with a glutamate side chain replacing the aspartate side chain: the expected mutation (see Fig. 2). The longer glutamate side chain at residue 141 repositions the carboxylate 1.9 Å further away from the guanidinium group of Arg108 and 1.5 Å closer to the edge of the heme (see Fig. 2). Despite the reorientation of the carboxylate, it remains just 2.8 Å from the main chain nitrogen of I237, although the change in geometry may have resulted in a slightly weaker hydrogen bond, consistent with the higher B values for the side chain atoms in Glu141 (B = 35–55 $Å^2$) compared with the native Asp141 side chain (B = 15–25 $Å^2$). The longer side chain also obstructs the binding of water molecule W5, but the remainder of the variant's structure and solvent distribution in the region is indistinguishable from the native structure. F2

The electron density maps of the D141E variant also differ from the maps of native BpKatG in the cavity containing the side chain of Arg426. The native structure at pH 5.6 has the Arg426 side chain distributed in two conformations, 30% associated with Tyr238 (conformation Y) and 70% shifted away (conformation R), whereas in variant D141E, the maps are consistent with approximately 80% of the side chain being in conformation Y. This is the predominant conformation found in KatG of *H. marismortui* and in crystals of BpKatG shifted to high pH.[20,32] To investigate if Arg426 remained sensitive to pH in variant D141E, a crystal was soaked in pH 8.0 buffer. As with the native enzyme, it survived the shift

J_ID: Z7E Customer A_ID: 21209 Cadmus Art: PROT21209 Date: 2-OCTOBER-06 Stage: I Page: 6

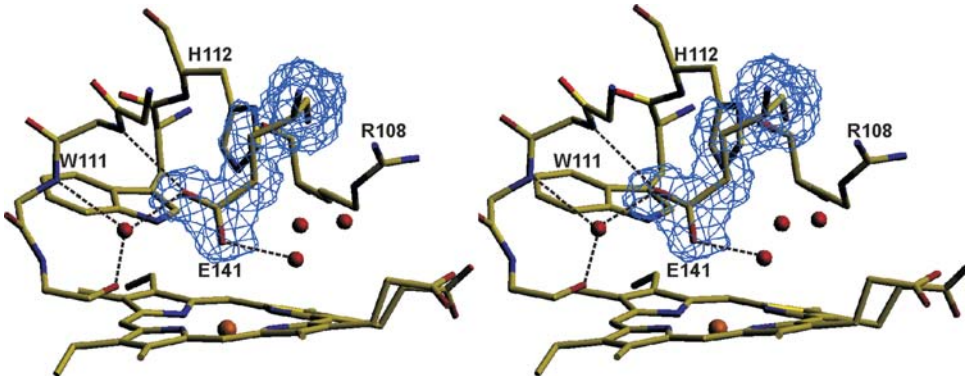

COLOR

Fig. 2. Stereo diagram showing the side chain of Glu141 and its corresponding electron density in the D141E variant. The $2F_o$–F_c electron density map drawn at $\sigma = 1.0$ corresponding to the Glu141 residue is drawn in blue. The waters are drawn in red.

in pH and the two major changes from the structure at pH 5.6 are consistent with changes observed in the native structure.[31] The Arg426 side chain changed to >95% conformation Y and the perhydroxy modification on Trp111, presumably associated with the oxidase reaction, appeared with 100% occupancy.

Structural Changes in the Heme Environment as Detected by 9-GHz EPR Spectroscopy

The correlation of data from X-ray crystallography and low temperature EPR spectroscopy has identified subtle, but significant, changes in the microenvironment of the heme active site of BpKatG, induced by variation of the solution pH between 4.5 and 8.5, which are directly related to changes in the enzyme activity.[32] Because many of the distal-side variants do not crystallize, the ferric EPR spectrum is an important tool with which to monitor the changes induced by the different mutations and to understand better the differences in enzyme activity.

The low temperature 9-GHz ferric EPR spectrum of the resting BpKatG (see Fig. 3) shows the contribution of two predominant signals, an axial signal (with $g_{A\perp} = 5.90$ and $g_{A\parallel} = 1.99$) in addition to a rhombically distorted signal ($g_{Bx} = 6.50$, $g_{By} = 5.10$ and $g_{Bz} = 1.97$), the ratio of intensities being pH dependent. At pH 5.6, the rhombically distorted signal B dominates the spectrum (see Fig. 3, solid trace). As previously described, the absence of the expected higher contribution of the axial signal A, in the ferric EPR spectrum at pH ≥7.5, is the result of the changes in the relative positioning of the iron, distal side waters, and the imidazole and indole nitrogens of His112 and Trp111, caused by the perhydroxy modification on Trp111.[32] Only the expansion of the spectrum showing the $g \cong 6$ resonance of these signals at the two pH values corresponding to the crystallization conditions is shown for clarity (see Fig. 3). The ferric EPR spectrum of the D141E variant at pH 8.0 is the same as that of the wild type enzyme (see Fig. 3) consistent with the presence of the perhydroxy modification on Trp111 observed in the crystal structure of this

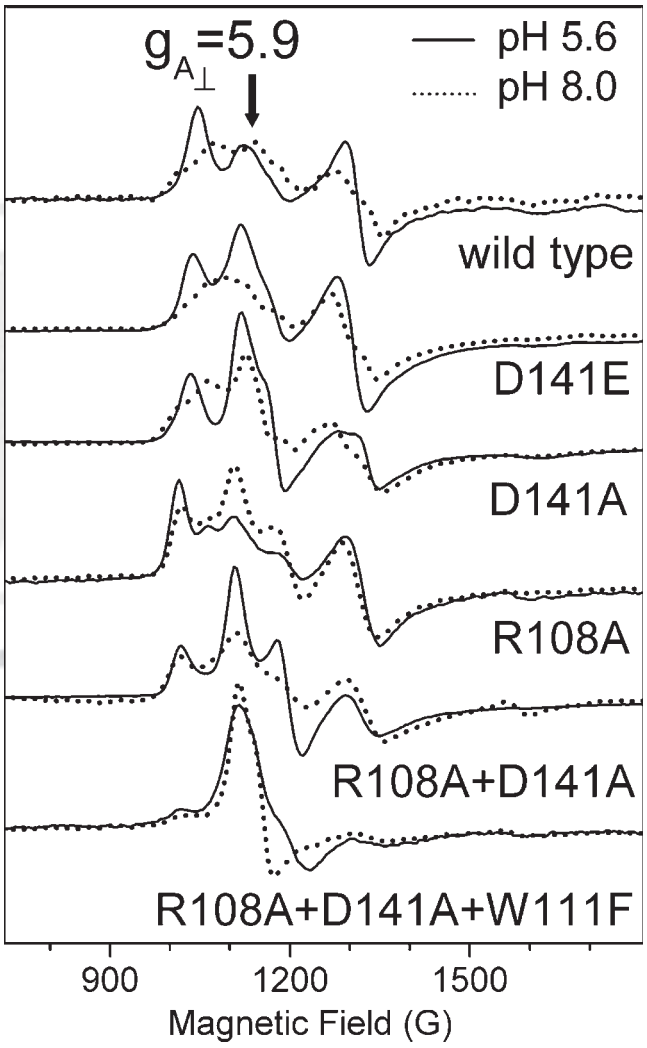

Fig. 3. The 9-GHz EPR spectra of wild-type, D141 and R108 variants of *B. pseudomallei* catalase–peroxidase in the resting (ferric) state and for the two optimum pH values for catalase-type (5.6) and oxidase-type (8.0) enzyme activities. Only the expansion of the $g \approx 6$ component of the typical (S/5) ferric heme iron spectrum is shown for clarity. All spectra were recorded at 4 K, 5-G modulation amplitude, 1-mW microwave power, 100-kHz modulation frequency.

J_ID: Z7E Customer A_ID: 21209 Cadmus Art: PROT21209 Date: 2-OCTOBER-06 Stage: I Page: 7

variant. At pH 5.6, a slightly higher contribution of the axial signal ($g_{A\perp} = 5.90$) is observed for the D141E variant, when compared with the wild type enzyme, an effect that can be explained by a mild repositioning of the distal side water(s) and the heme iron. Accordingly, the crystal structure of the D141E variant at pH 5.6 shows longer W4-to-iron distance (2.75 Å in subunit A or 3.04 Å in subunit B), when compared with the wild type enzyme (2.46 Å in subunit A or 2.55 Å in subunit B). Such a mild change has little influence on the catalase activity (Table II). By contrast, the ferric EPR spectrum of the D141A variant at pH 5.6 exhibits a predominant axial signal similar to the Y238F and W111F variants.[32] This is consistent with a more dramatic change in the positioning of water(s) in close proximity to the heme iron, and as for variants Y238F and W111F, the change in variant D141A is associated with a 95% loss of catalase activity.

A different effect is observed in the in Arg108 variants such as the R108A variant, in which the ferric EPR spectrum shows a measurable difference in the rhombic distortion of the signal, when compared with the wild-type spectrum ($g_{Bx} = 6.61$, $g_{By} = 5.08$ and $g_{Bz} = 1.96$) with no pH-dependence of the signals (see Fig. 3). Arg108 is further away from the perpendicular direction to the heme plane, even though it interacts with the iron through an extended H-bonding network as previously demonstrated for SyKatG.[8] Accordingly, the changes in the EPR spectrum are consistent with the 66% decrease in catalase activity of this variant, when compared with the wild-type enzyme (Table II).

The spectral changes observed in the ferric EPR spectrum of the double variant R108A/D141A appear to be a combination of the changes induced by the individual mutations, that is, a predominant axial signal as in variant D141A and a higher rhombic distortion on signal B with no pH dependence as in variant R108A (see Fig. 3). Considering the structural changes predicted by the spectra, an almost complete loss of catalase activity in the D141A/R108A variant was anticipated, whereas the observed activity is only 18% lower than the wild-type enzyme. This clearly indicates that although the mutations do not restore the relative positioning of the waters and distal side residues of the wild type enzyme [Fig. 1(b)], the new configuration adopted in the R108A/D141A variant is favorable for H_2O_2 binding and catalase function. It is of note that all W111F-containing variants (W111F, R108A/W111F and R108A/D141A/W111F) exhibit a predominant axial signal A for all pH values (see Fig. 3) and this agrees well with the almost 100% loss of the catalase activity in all cases.

DISCUSSION

A number of possible roles for Asp141 have been suggested including a direct involvement in the catalytic deprotonation of H_2O_2 during the reduction of compound I, creation of an electrical potential in conjunction with the positively charged heme iron that acts on the electrical dipoles of solvent and substrate in the channel, enhancement of the iron (proximal imidazole bond strength), modification of the coordination state of the iron, and modification of the protonation state of His112.[22] The first of these possibilities, a direct catalytic role for Asp141, is unlikely for two reasons. First, the R108A/D141A double variant which lacks the carboxylate exhibits near normal catalase activity and, second, the carboxylate side chain is relatively rigidly positioned by a short and presumably strong 2.7 Å hydrogen bond to the main chain nitrogen of Ile237. The location and geometry of the sp^2 orbitals of a carboxylate group limit the range of its interactions, and the hydrogen bonds with waters, W1, W2, and W6, and the Ile237 nitrogen in the native and compound I structures exhibit appropriate geometry. Thus, for Asp141 to play a catalytic role in the deprotonation of H_2O_2 associated with the hydroxoferryl heme group in the heme cavity,[21,22] the carboxylate group would have to rotate and reorient the sp^2 orbitals, breaking at least transiently the existing hydrogen bonds including that with the main chain nitrogen of Ile237, and this is not supported by any structural evidence.

The suggestion that Asp141 creates an electrical potential field in conjunction with the heme iron to act on the electrical dipoles of incoming substrate and solvent to facilitate hydrogen bonding can be questioned. This particular concept was proposed for monofunctional catalases,[33] but in those enzymes the orientation of the aspartate is only 5° from the perpendicular to the plane of the heme, whereas in KatGs, the residue 141 carboxylate creates a 45° with the iron in the plane of the heme. Furthermore, if a potential field effect is operating in KatGs, it must require the presence of Arg108, but the proximity of the positively charged Arg108 side chain to Asp141 should actually reduce or distort the field. Further complicating the involvement of a potential field as a catalytic determinant is the fact that the K_m for H_2O_2 in the catalase reaction is elevated in both the R108A/D141A variant, where the carboxylate is absent, and the D141E variant, where the carboxylate is present. Similarly, the importance of the heme coordination state and the proximal iron–imidazole bond strength to the catalase reaction must be small because of the near normal catalase activity of the R108A/D141A variant.

What then is the role of Asp141 in the catalase reaction? This can be explained well in terms of the precise juxtaposition of Asp141 and Arg108, which creates substrate binding sites that control entry of the substrate into the heme cavity by one of two paths. The branches of water leading from W1 [Fig. 1(b)] to the heme iron clearly delineate the paths with one branch leading to the catalytic site between Arg108 and His112 and the second leading to the catalytic site between Trp111 and His112. The importance of this water matrix in the catalase reaction has been previously demonstrated[22,34] and the role of Asp141 and Arg108 in matrix stabilization is confirmed in this work (see Fig. 3). The role of the charged side chains of Arg108 and Asp141 is to present

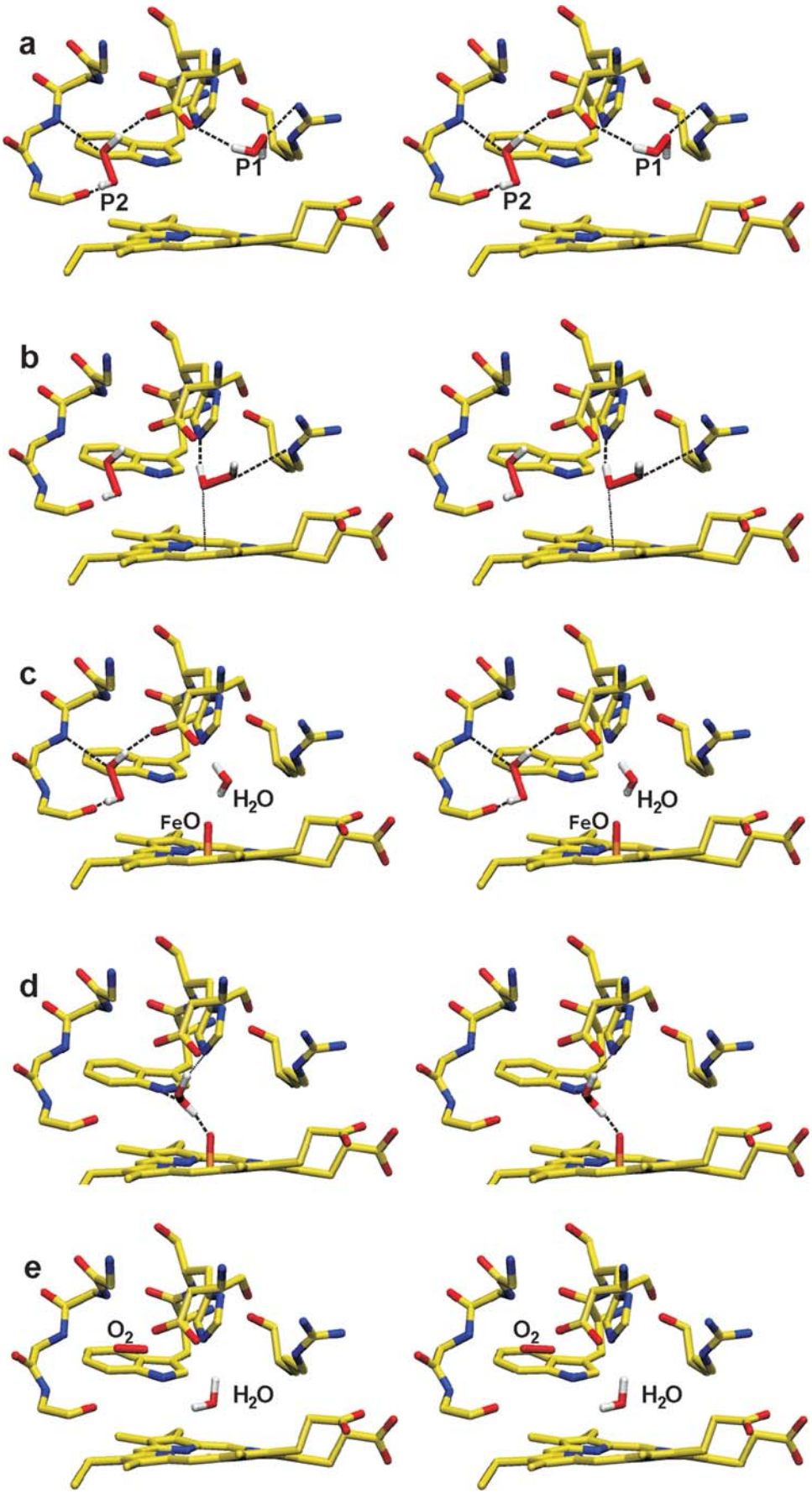

COLOR

Fig. 4. Stereo diagrams depicting a series of binding sites for H_2O_2 entering the heme active site. In panel (**a**), two substrate molecules are shown bound at sites P1, between Asp141 and Arg108, and P2, among Asp141 and the main chain atoms of residues 238 and 239. In panel (**b**), the H_2O_2 has moved so that it is interacting with Arg108 and His112 prior to formation of compound I and water shown in panel (**c**). The thinner line between the H_2O_2 and iron in panel (**b**) denotes a weak interaction that is just starting to form. Panel (**d**) shows the second H_2O_2 having moved from P2 to interact with Trp111 and His112 prior to reduction of compound I giving the products shown in panel (**e**).

J_ID: Z7E Customer A_ID: 21209 Cadmus Art: PROT21209 Date: 2-OCTOBER-06 Stage: I Page: 9

strong interaction sites for H_2O_2 and this is evident in the properties of the variants. Removal of Asp141, as in D141A, allows the incoming substrate to bind only with Arg108 leading to binding in the Arg108–His112 catalytic site for heme oxidation and compound I formation. Compound I reduction is less favorable because H_2O_2 interaction with Arg108 continues to retard movement of the substrate to the Trp111–His112 catalytic site. Removal of Arg108, as in R108A, not only eliminates the Arg108–His112 catalytic site but allows the substrate to bind mainly with Asp141. This slows its movement to the Trp111–His112 catalytic site, which can now be used for both compound I formation, albeit not as efficiently, and compound I reduction. Simultaneous removal of Arg108 and Asp141 eliminates both strong substrate binding residues allowing the substrate to enter the Trp111–His112 catalytic active site more easily for both compound I formation and reduction.

The first branch of solvent passes between the side chains of Asp141 and Arg108, where the separation between the carboxylate and guanidinium groups is too great for simultaneous hydrogen bonding with the same water (see Fig. 1). However, the distance and orbital geometry accommodate an H_2O_2 very well (see Fig. 4) in the absence of waters W1 and W2. This binding site, labeled P1, should slow H_2O_2 movement into the Arg108–His112 catalytic site for compound I formation, consistent with the higher K_m for compound I formation when the aspartate is present (Table II). On the other hand. removal of the carboxylate, as in D141A, or even moving it 1.9 Å further away from Arg108, as in D141E, prevents H_2O_2 binding at P1, thereby allowing less obstructed access to the Arg108–His112 site consistent with the reduced K_m for H_2O_2 in compound I formation (Table II). Beginning with P1, a series of possible binding sites for H_2O_2 between P1 and the Arg108–His112 catalytic site leading to compound I formation can be modeled [Fig. 4, panels (a–c)]. An extended series of binding sites is available in the Supplementary material [Fig. S1(A)].

The second branch of solvent leading into the heme cavity begins with W5 which, despite its proximity to the Asp141 carboxylate, is positioned to create a favorable hydrogen bond with only one carboxylate oxygen and then only if the hydrogen bonds with waters W1 and W2 are broken. However, as part of the water matrix, W5 is hydrogen bonded between W1 and W6, and W6 is favorably situated to hydrogen bond with the carboxylate of Asp141, the main chain carbonyl oxygen of Val239 and the main chain nitrogen of Tyr238. Displacement of W6 provides a favorable binding site for H_2O_2, labeled P2 (see Fig. 4), involving the same three hydrogen bonds placing the substrate on the solvent path leading to the Trp111–His112 catalytic site for compound I reduction. The involvement of Asp141 as a facilitator of this reaction is in agreement with the decreased K_m for compound I reduction in the presence of Asp141 (Table II). A series of possible binding sites for H_2O_2 between P2 and the Trp111–His112 catalytic site leading to compound I reduction can be modeled [Fig. 4, panels (c–e)]. An extended series of binding sites is available in the Supplementary material [Fig. S1(B)].

The kinetic properties of variant D141E including a lower K_m for H_2O_2 in compound I formation and a higher K_m for H_2O_2 in the catalatic compound I reduction compared with the native protein provide yet another indication of how sensitive the catalase reaction is to subtle structural changes in the protein. The small change in location of the carboxylate of Glu141 places it too far from Arg108 to allow participation in the binding of H_2O_2 at P1. This allows easier access of substrate to the Arg108–His112 catalytic site and a more facile compound I formation. The reason for more difficult catalatic compound I reduction in D141E is not as clear and could be a result of the longer glutamate chain constricting the entrance channel, enhancing electron density on the heme, binding H_2O_2 more poorly at P2, and allowing more H_2O_2 binding at Arg108–His112.

CONCLUSIONS

Although catalase activity is significantly diminished in all the single variants of Asp141 except D141E, simultaneous removal of Arg108, as in the double variant D141A/R108A, restores catalase activity to near native levels. It is postulated that Asp141 promotes catalase activity in the presence of Arg108 by creating a binding site for substrate H_2O_2 that competes with binding between Arg108 and His112. Inside the distal heme pocket, the solvent is organized in two paths, one between Arg108 and Asp141, and the second between Asp141 and the main chain atoms of residues 237–239. The movement of substrate H_2O_2 into the active site is controlled by binding either between Arg108 and Asp141, which slows its movement to the Arg108–His112 catalytic site for compound I formation or between Asp141 and the main chain atoms of residues 237 and 239, which directs it towards the Trp111–His112 catalytic site for compound I reduction. Other subtle changes such as the closer proximity of the carboxylate to the heme, constriction of the entrance channel by the longer side chain of Glu141 and shift in the equilibrium of Arg426 to greater interaction with Tyr238 contribute to the kinetic properties of the catalase reaction of the D141E variant. The 9-GHz EPR spectrum of the native enzyme clearly demonstrates the complexity of the relationship between activity and the three-dimensional arrangement of the water matrix and distal side residues in KatGs and provides additional support for the concept of and relevance for catalytic activity of the extended H-bonding network.

REFERENCES

1. Klotz MG, Loewen PC. The molecular evolution of catalatic hydroperoxidases: evidence for multiple lateral transfer of genes between prokaryota and from bacteria into eukaryota. Mol Biol Evol 2003;20:1098–1112.
2. Singh R, Wiseman B, Deemagarn T, Donald LJ, Duckworth HW, Carpena X, Fita I, Loewen PC. Catalase–peroxidases (KatG) exhibit NADH oxidase activity. J Biol Chem 2004;279: 43098–43106.

3. Zhang Y, Heym B, Allen B, Young D, Cole S. The catalase–peroxidase gene and isoniazid resistance of *Mycobacterium tuberculosis*. Nature 1992;358:591–593.
4. Rozwarski DA, Grant GA, Barton DHR, Jacobs WR, Sacchettini JC. Modification of the NADH of the isoniazid target (InhA) from *Mycobacterium tuberculosis*. Science 1998;279:98–102.
5. Lei B, Wei CJ, Tu SC. Action mechanism of antitubercular isoniazid: activation by *Mycobacterium tuberculosis* KatG, isolation and characterization of InhA inhibitor. J Biol Chem 2000;275: 2520–2526.
6. Wilming M, Johnsson K. Spontaneous formation of the bioactive form of the tuberculosis drug isoniazid. Angew Chem Int Ed Engl 1999;38:2588–2590.
7. Mdluli K, Slayden RA, Zhu Y, Ramaswamy S, Pan X, Mead D, Crane DD, Musser JM, Barry CE. Inhibition of a *Mycobacterium tuberculosis* ∃-ketoacyl ACP synthase by isoniazid. Science 1998;280:1607–1610.
8. Ivancich A, Jakopitsch C, Auer M, Un S, Obinger C. Protein-based radicals in the catalase-peroxidase *Synchocystis* PCC6803: a multifrequency EPR investigation of wild-type and variants on the environment of the heme active site. J Am Chem Soc 2003;125:14093–14102.
9. Welinder KG. Superfamily of plant, fungal and bacterial peroxidases. Curr Opin Struct Biol 1992;2:388–393.
10. Yamada Y, Fujiwara T, Sato T, Igarashi N, Tanaka N. The 2.0 Å crystal structure of catalase-peroxidase from *Haloarcula marismortui*. Nat Struct Biol 2002;9:691–695.
11. Carpena X, Loprasert S, Mongkolsuk S, Switala J, Loewen PC, Fita I. Catalase-peroxidase KatG of *Burkholderia pseudomallei* at 1.7 Å resolution. J Mol Biol 2003;327:475–489.
12. Wada K, Tada T, Nakamura Y, Kinoshita T, Tamoi M, Sigeoka S, Nishimura K. Crystallization and preliminary X-ray diffraction studies of catalase-peroxidase from Synechococcus PCC7492. Acta Crystallogr D 2002;58:157–159.
13. Bertrand T, Eady NAJ, Jones JN, Nagy JM, Jamart-Grégoire B, Raven EL, Brown KA. Crystal structure of *Mycobacterium tuberculosis* catalase–peroxidase. J Biol Chem 2003;279:38991–38999.
14. Hillar A, Peters B, Pauls R, Loboda A, Zhang H, Mauk AG, Loewen PC. Modulation of the activities of catalase-peroxidase HPI of *Escherichia coli* by site-directed mutagenesis. Biochemistry 2000;39:5868–5875.
15. Regelsberger G, Jakopitsch C, Ruker F, Krois D, Peschek GA, Obinger C. Effect of distal cavity mutations on the formation of compound I in catalase–peroxidases. J Biol Chem 2000;275:22854–22861.
16. Deemagarn T, Carpena X, Singh R, Wiseman B, Fita I, Loewen PC. Structural characterization of the Ser324Thr variant of the catalase–peroxidase (KatG) from *Burkholderia pseudomallei*. J Mol Biol 2005;345:21–28.
17. Jakopitsch C, Auer M, Ivancich A, Ruker F, Furtmuller PG, Obinger C. Total conversion of bifunctional catalase–peroxidase (KatG) to monofunctional peroxidase by exchange of a conserved distal side tyrosine. J Biol Chem 2003;278:20185–20191.
18. Jakopitsch C, Ivancich A, Schmuckenschlager F, Wanasinghe A, Pöltl G, Furtmüller P, Rükert F, Obinger C. Influence of the unusual covalent adduct on the kinetics and formation of radical intermediates in Synechocystis catalase peroxidase. J Biol Chem 2002;279:46082–46095.
19. Yu S, Girotto S, Zhao X, Magliozzo RS. Rapid formation of compound II and a tyrosyl radical in the Y229F mutant of *M. tuberculosis* KatG disrupts catalase but not peroxidase function. J Biol Chem 2003;278:44121–44127.
20. Carpena X, Wiseman B, Deemagarn T, Singh R, Switala J, Ivancich A, Fita I, Loewen PC. A molecular switch and electronic circuit modulate catalase activity in catalase–peroxidases. EMBO Rep 2005;6:1156–1162.
21. Jakopitsch C, Auer M, Regelsberger G, Jantschko W, Furtmuller PG, Ruker F, Obinger C. Distal site aspartate is essential in the catalase activity of catalase–peroxidases. Biochemistry 2003; 42:5292–5300.
22. Jakopitsch C, Droghetti E, Schmuckenschlager F, Furtmuller PG, Smulevich G, Obinger C. The role of the main access channel of catalase–peroxidase in catalysis. J Biol Chem 2005;280: 42411–42422.
23. Otwinowski Z, Minor W. Processing of X-ray diffraction data collected in oscillation mode. Methods Enzymol 1996;276:307–326.
24. Murshudov GN, Vagin AA, Dodson EJ. Refinement of macromolecular structures by the maximum-likelihood method. Acta Crystallogr D 1997;53:240–255.
25. Jones TA, Zou JY, Cowan SW, Kjeldgaard M. Improved methods for building protein models in electron density maps. Acta Crystallogr A 1991;47:110–119.
26. Evans S. SETOR: hardware lighted three-dimensional solid model representations of macromolecules. J Mol Graph 1993;11: 134–138.
27. Humphrey W, Dalke A, Schulten K. VMD–visual molecular dynamics. J Mol Graph 1996;14:33,34.
28. Rorth HM, Jensen PK. Determination of catalase activity by means of the Clark electrode. Biochim Biophys Acta 1967; 139:171–173.
29. Childs RE, Bardsley WG. The steady-state kinetics of peroxidase with 2,20-azino-di-(3-ethyl-benzthiazoline-6-sulphonic acid) as chromagen. Biochem J 1975;145:93–103.
30. Layne E. Spectrophotometric and turbidimetric methods for measuring proteins. Methods Enzymol 1957;3:447–454.
31. Wang Y, Margoliash E. Enzymic activities of covalent 1:1: complexes of cytochrome c and cytochrome c peroxidase. Biochemistry 1995;34:1948–1958.
32. Carpena X, Wiseman B, Deemagarn T, Herguedas B, Ivancich A, Singh R, Loewen PC, Fita I. Roles for Arg426 and Trp111 in the modulation of NADH oxidase activity of the catalase–peroxidase KatG from *Burkholderia pseudomallei* inferred from pH-induced structural changes. Biochemistry 2006;45:5171–5179.
33. Chelikani P, Carpena X, Fita I, Loewen PC. An electrical potential in the access channel of catalases enhances catalysis. J Biol Chem 2003;278:31290–31296.
34. Jakopitsch C, Obinger C, Un S, Ivancich A. Identification of Trp106 as the tryptophanyl radical intermediate in *Synechocystis* PCC6803 catalase–peroxidase by multifrequency electron paramagnetic resonance spectroscopy. J Inorg Biochem 2006; 100:1091–1099.